Additive Effect on Reductive Decomposition and Binding of Carbonate-Based Solvent toward Solid Electrolyte Interphase Formation in Lithium-Ion Battery

Keisuke Ushirogata,[†,‡] Keitaro Sodeyama,[#,‡] Yukihiro Okuno,*[,†,‡] and Yoshitaka Tateyama*[,‡,#,∥]

[†]Research and Development Management Headquarters, FUJIFILM Corporation, 210 Nakanuma, Minamiashigara, Kanagawa 250-0193, Japan

[‡]International Center for Materials Nanoarchitectonics (MANA), National Institute for Materials Science (NIMS), 1-1 Namiki, Tsukuba, Ibaraki 305-0044, Japan

[#]Elements Strategy Initiative for Catalysts & Batteries, Kyoto University, Goryo-Ohara, Nishikyo-ku, Kyoto 615-8245, Japan

[∥]PRESTO and CREST, Japan Science and Technology Agency (JST), 4-1-8 Honcho, Kawaguchi, Saitama 333-0012, Japan

S *Supporting Information*

ABSTRACT: The solid−electrolyte interphase (SEI) formed through the reductive decomposition of solvent molecules plays a crucial role in the stability and capability of a lithium-ion battery (LIB). Here we investigated the effects of adding vinylene carbonate (VC) to ethylene carbonate (EC) solvent, a typical electrolyte in LIBs, on the reductive decomposition. We focused on both thermodynamics and kinetics of the possible processes and used density functional theory-based molecular dynamics with explicit solvent and Blue-moon ensemble technique for the free energy change. We considered Li^+ in only EC solvent (EC system) and in EC solvent with a VC additive (EC/VC system) to elucidate the additive effects. In addition to clarifying the equilibrium properties, we evaluated the free energy changes along several EC or VC decomposition pathways under one-electron (1e) reduction condition. Two-electron (2e) reduction and attacks of anion radicals to intact molecules were also examined. The present results completely reproduce the gaseous products observed in the experiments. We also found a new mechanism involving the VC additive: the VC additive preferentially reacts with the EC anion radical to suppress the 2e reduction of EC and enhance the initial SEI formation, contrary to the conventional scenario in which VC additive is sacrificially reduced and its radical oligomerization becomes the source of SEI. Because our mechanism needs only 1e reduction, the irreversible capacity at the SEI formation will decrease, which is also consistent with the experimental observations. These results reveal the primary role of VC additive in the EC solvent.
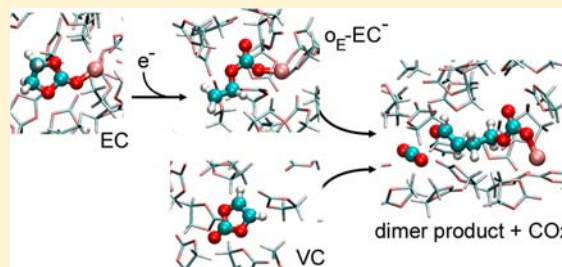
1. INTRODUCTION

Rechargeable lithium-ion batteries (LIBs) have been widely used in portable electronics and, because of their high-energy storage characteristics, are now being applied in more critical applications such as electric and hybrid vehicles, medical devices, and power storage systems in smart grids. For such future use, a higher degree of safety, a longer cycle life, and the ability to operate under higher voltage are required.[1,2] Many studies on LIBs have been carried out in the past decades to address these concerns.[1−36]

A crucial key to the LIB stability and durability is the performance of the solid−electrolyte interphase (SEI).[2,4−36] At the first charging, reductive decomposition of the electrolyte occurs to generate the sources of the SEI. These lie down at the negative electrode interfaces, leading to the growth of the SEI film. Once formed, the SEI hinders electron tunneling from the electrode and thus prevents further electrolyte decomposition, while still allowing Li^+ to diffuse between the electrolyte and the electrode. The robustness and efficiencies of the SEI thus significantly affect the power capability, safety, and cycle life of a

LIB. In a typical LIB setup, the electrolyte consists of lithium salts (e.g., $LiPF_6$) and cyclic alkyl carbonates, e.g., ethylene carbonate (EC), as shown in Figure 1, with linear carbonates (e.g., dimethyl carbonate) to decrease the melting point and viscosity. The decomposition products of the EC solvents are regarded as main components of the SEI film.[8] However, a
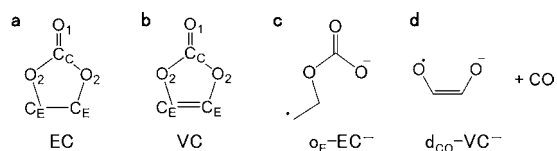

Figure 1. (a,b) Structures of EC and VC with the labels used throughout this paper. (c,d) Major reductive decomposition products of EC and VC, which are labeled o_E-$EC^−$ and d_{CO}-$VC^−$, respectively, in this paper.

thorough understanding of even this fundamental process is still lacking. The microscopic mechanism responsible for the reductive decomposition and subsequent growth of the SEI is unclear because of the difficulty in the in situ observation of the electrode−electrolyte interface in the LIB.

Additives to the electrolyte also have a large impact on the SEI formation mechanism and its performance. An example is vinylene carbonate (VC, Figure 1) additive to the EC solvent.[11] Even a small amount of VC up to 5−10% significantly improves the irreversible capacity at the first charging and the cycle life of lithium-ion polymer cells.[10,14,16] A proposed mechanism is that VC additives are sacrificially reduced and decomposed on behalf of EC and form the oligomer structures, leading to the improved SEI.[10,22] However, the solvation properties of VCs with respect to Li^+ as well as the subsequent decomposition processes have not yet been established on the atomic scale. An atomistic investigation of the role of VC additives in SEI formation is therefore crucial for an in-depth understanding of LIB durability and performance.

Quantum mechanical calculations based on density functional theory (DFT) are useful for examining such molecular reactions on an atomic scale. There have been, in fact, many studies of reductive decomposition in LIBs. A typical approach is a DFT quantum chemistry calculation of the Li^+ ion and some solvent molecules with or without a dielectric continuum approximation of the liquid environment.[21−31] In particular, Balbuena and co-workers examined the reductive decomposition of solvated EC and EC/VC molecules solvated to Li^+.[21−23] Though possible reaction pathways have been proposed from these calculations with cluster boundary conditions (CBC), consideration of the explicit solvents as well as dynamics is still indispensible for substantial understanding of the solvation dynamics and the estimation of free energy changes, including the entropy effects.

To address this need, Leung and co-workers recently carried out DFT-based molecular dynamics (DFT-MD) studies with explicit solvent, although still computationally demanding.[32−36] These authors investigated the decomposition mechanism of the EC solvent and concluded that the EC decomposition is dominated by two-electron (2e) reductions at the electrode−electrolyte interface, not the one-electron (1e) reductions that have been the focus of the traditional quantum chemical calculations.[21−23] Furthermore, Leung et al. showed the generation of the gases CO and C_2H_4 from the reduction of the EC solvent. Although these studies provided many aspects, they mainly discussed the observation of spontaneous processes in the DFT-MD simulations. Information about barriers and the kinetics of the decomposition processes was therefore not fully considered.

In this study, we investigated the thermodynamics as well as the kinetics of the reductive decomposition of the electrolyte, by using standard DFT-MD sampling and the Blue-moon ensemble technique. The latter method enables us to calculate the free energy profile including entropy effects, and thus elucidate possible decomposition and binding mechanisms in more detail. We dealt with the Li^+ in the EC solvent only (EC system) and that in the EC solvent with the VC additive (EC/VC system) to elucidate the additive effect on the initial process of the SEI formation. After clarifying the equilibrium structural and electronic properties, we evaluated the free energy change along several EC or VC decomposition pathways under the 1e and 2e reduction conditions. Attacks of the resulting anion radicals to intact molecules were also examined. On the basis of

all the results, we discuss the formation of the gaseous products during the decomposition of the electrolyte and compare our results with available experimental data. Finally we suggest a new insight into the reductive decomposition mechanism leading of these molecules toward the SEI formation.

2. CALCULATIONS

2.1. Model System. The SEI usually forms on the interface between the electrolyte and negative electrode at the charging stage. The electronic potential at the electrode is low enough (around 0 V vs Li/Li^+) for its electron to transfer easily to the solvent molecules near the interface. This reductive electron transfer can initiate the solvent decomposition. As a simplest model of this situation, we adopted a supercell approach (Figure 2). The supercell involves Li^+, the EC
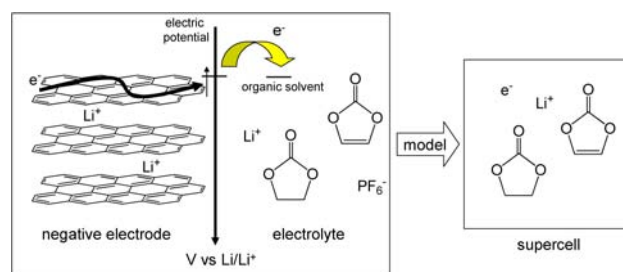

Figure 2. Schematic description of supercell calculation model of the reductive decomposition near the negative electrode.

solvent, and the VC additive, if necessary, with the transferred electrons only without the electrode to save the computational cost. We also excluded counter-anions of the Li salt (e.g., PF_6^-) because they are less likely to be near the negative electrode at the charging stage. We believe that this approach provides a reasonable description of the reductive decomposition and binding of EC and VC, the initial processes of the SEI formation.

For the 1e reduction, we used the supercell with one Li atom under neutral charge condition. Because the Li atom immediately transforms to a Li^+ cation, one electron is transferred to a solvent or additive molecule, the results being the 1e reduction condition. Introduction of another Li atom in the supercell can make the 2e reduction system. However, the present supercell is not large enough to describe the solvation shells of two Li^+. We therefore used an alternative way of −1e charged supercell for the 2e reduction case. The periodic boundary condition (PBC) used here introduces the homogeneous background charge to make the system formally neutral. In this way, we can deal with the reduction reactions in the electrolyte while taking into account the solvation shells via the explicit solvent molecules.

2.2. DFT Molecular Dynamics. The supercells include 32 EC molecules (EC system) or 31 EC and one VC (EC/VC system) with or without one Li atom. The 1e and 2e reduction systems are prepared as described above. We also used a +1e charged supercell for the equilibrium states before the reduction occurs. The cubic box with a length of 15.24 Å is used for the supercell to reproduce EC density of 1.32 g/cm^3.[24,25,32] The PBC is adopted to deal with the liquid state at constant density. We carried out DFT-MD simulations in the framework of Car−Parrinello dynamics,[37] by using CPMD code.[38] A fictitious electronic mass of 600 au and a time step of 5 au (0.12 fs) were chosen. The system temperature was controlled using a Nosé thermostat[39] with a target temperature of 353 K. After equilibration, statistical averages were computed from trajectories of at least 3 ps in length. The electronic wave function was quenched to the Born−Oppenheimer surface about every 1 ps in order to maintain adiabaticity. We used the PBE exchange-correlation functional. The energy cutoff of the plane wave basis set is set to 90 Ry. Stefan Goedecker's norm-conserving pseudopotentials for C, H, O, and Li were used.[40−42] Some calculations were carried out in the local spin density (LSD) approximation.

2.3. Blue-Moon Ensemble. The free energy profiles of the decomposition processes were evaluated with the Blue-moon ensemble technique.[43] We chose the distances of C_C-O_2 and C_E-O_2 (Figure 1) as well as their combinations as the reaction coordinates (ξ') of the decomposition processes. Constrained DFT-MD simulations were carried out for about 10 values of ξ' between the initial (ξ_a) and the final (ξ_b) states of the processes to obtain the set of potentials of mean force (PMFs), $dA/d\xi'$. The PMF is written as

$$\frac{dA}{d\xi'} = \langle -\lambda \rangle_{\xi'}$$

where λ is the Lagrange multiplier of the constrained DFT-MD. We then constructed the free energy profiles by integrating the PMFs from the initial reaction coordinate:

$$A(\xi_b) - A(\xi_a) = \int_{\xi_a}^{\xi_b} d\xi' \frac{dA}{d\xi'}$$

Note that we sometimes constructed the profile $A(\xi)$ just until the transition state when the additional processes appeared in the constrained DFT-MD. These are still relevant for the discussion of kinetics.

2.4. Analysis with DFT Cluster Boundary Calculations. Statistical properties of the equilibrium and transition states were estimated via DFT-MD with PBC, while the local cluster analysis of the solvation shell was carried out by DFT and hybrid-DFT methods with CBC as implemented in Gaussian 09.[44] This enabled us to evaluate molecular properties more clearly and check the functional dependence. The exchange and correlation functionals used were B3LYP[45] and PBE[46,47] with a 6-311++G(d,p) basis set, and the geometries were fully optimized. In the analyses, the solvent effect was dealt with using the polarized continuum model (PCM) method with the parameters for EC bulk solvent (dielectric constant $\varepsilon = 89.78$).

3. RESULTS AND DISCUSSION

3.1. Solvation Structure to Li$^+$. We first examined the solvation properties of EC and EC/VC systems on Li$^+$ without excess electrons. It is well known that Li$^+$ prefers four-fold tetrahedral coordination in a carbonate solvent. Both EC and EC/VC systems in the present calculations exhibited such four-fold coordinated structures. For the EC/VC system, we treated two types of initial coordination: Li coordinated with four EC (Li-4EC) and Li coordinated by three EC and one VC (Li-3EC1VC). The average total energies of their equilibrium trajectories indicated that the Li-4EC solvation is more stable than the Li-3EC1VC by 9.6 kcal/mol. Furthermore, in the DFT-MD simulation of the Li-3EC1VC system, we eventually observed exchange from VC to EC in the first solvation shell to Li$^+$, resulting in the Li-4EC system. Therefore, the additive VC molecules prefer not solvating to Li$^+$ in the EC solvent at equilibrium (see Supporting Information Figure S1). Population analysis with the CBC calculations (PBE/6-311++G(d,p)) indicates that the total charges of the CO$_3$ part of EC and VC are estimated as −0.68e and −0.58e, respectively. This difference in total charge accounts for the larger interaction of EC than VC with the Li$^+$, and it is consistent with the HSAB rule for hard acid (see Supporting Information Table S1).

3.2. One-Electron (1e) Reductive Decomposition. Next we introduced one excess electron into the supercell. We put the excess electron into EC coordinating to Li$^+$ in the EC system (EC$^-$-Li$^+$), VC coordinating to Li$^+$ in the EC/VC system (VC$^-$-Li$^+$), and VC not coordinating to Li$^+$ in the EC/VC system (VC$^-$) in the initial structures of DFT-MD samplings. The average energy difference between the systems before and after receiving the electron suggests that VC$^-$-Li$^+$ is

more stable than EC$^-$-Li$^+$ by 6.7 kcal/mol. In the case of VC$^-$ apart from Li$^+$, the excess electron transfers from VC to EC coordinating to Li$^+$ immediately in the simulation. Therefore, we conclude that the order of anion molecule stability is VC$^-$-Li$^+$ > EC$^-$-Li$^+$ > VC$^-$. This is consistent with the order of electron affinity in the CBC calculations (see Supporting Information Table S2). Note that no spontaneous decomposition was observed during these DFT-MD samplings, indicating the importance of kinetic information to elucidate the decomposition processes.

We then carried out constrained MD in the framework of Blue-moon ensemble for the decomposition reaction barriers. The 1e reduction decomposition of the EC system was investigated first. Here we applied two pathways for the ring-opening, shown as (1) and (2) in Scheme 1, to one of the

Scheme 1. One-Electron (1e) Reductive Decomposition Reactions
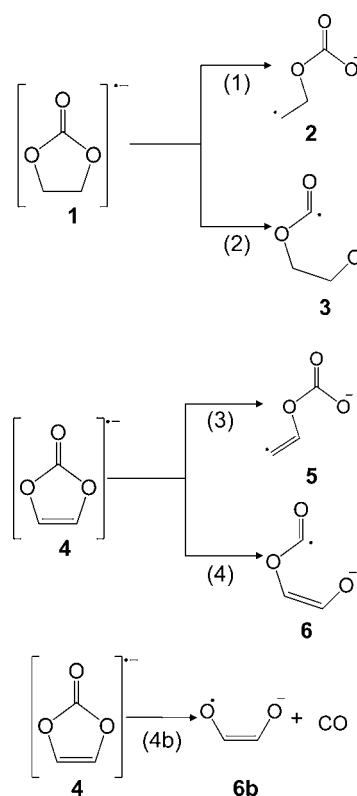
solvated ECs. The calculation constraints, ξ, were set to the sum of both C_E-O_2 bond distances and one of C_C-O_2 bond distance, respectively. In case (1), we initially used the distance of only one C_E-O_2 bond as the constraint but observed that the other unconstrained C_E-O_2 bond dissociates together toward an artifact product with higher energy. For that reason, we chose the sum of the C_E-O_2 bond distances as the constraint for path (1). Figure 3a shows the resultant free energy profiles with respect to $\Delta\xi$ (difference of ξ from ξ_{eq} in the initial structure). We have taken the free energy associated with distances 2.9 Å (the sum of equilibrium bond distances of C_E-O_2) and 1.5 Å (the equilibrium C_C-O_2 bond distance) as the zero reference energy for the C_E-O_2 and C_C-O_2 bond-breaking cases, respectively.

From Figure 3a, we can estimate the activation and reaction energies of path (1) to be 4.8 and −24.5 kcal/mol, respectively.
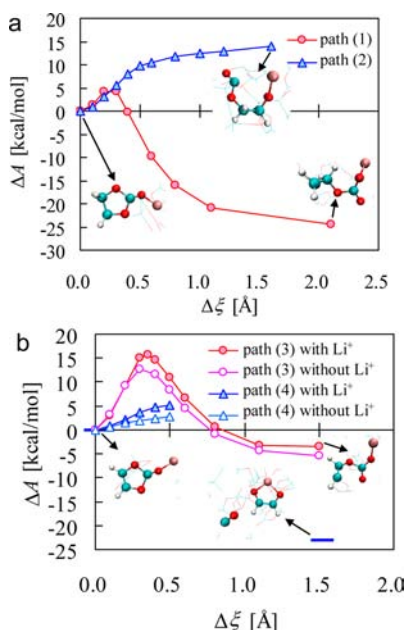
Figure 3. Free energy profiles, ΔA, of one-electron reductive decomposition along the mechanical constraint ξ. (a) ΔA of paths (1) and (2) in Scheme 1 with constraint $\Delta\xi = r(C_E-O_2) + r(C_E-O_2) - (r_{eq}(C_E-O_2) + r_{eq}(C_E-O_2))$ and $\Delta\xi = r(C_C-O_2) - r_{eq}(C_C-O_2)$, respectively, where r_{eq} is the equilibrium bond distance of the initial state. (b) ΔA of paths (3) and (4) with mechanical constraint $\Delta\xi = r(C_E-O_2) - r_{eq}(C_E-O_2)$ and $\Delta\xi = r(C_C-O_2) - r_{eq}(C_C-O_2)$, respectively. In (b), we show the results of paths for VC coordinated (with Li^+)/uncoordinated (without Li^+) to the Li atom. The blue bars indicate the average total energies of reactant, VC^-, and a most stable product, CO and d_{CO}-VC^-, for comparison.

In contrast, the free energy profile along path (2) increases monotonically with an increase of the constraint. The reaction along path (2) is therefore unfavorable in our calculated results. On this C_C-O_2 bond cleavage, a previous study based on a cluster model calculation of $(Li^+\text{-}EC^-)$[27] showed that there is a stable C_C-O_2 bond cleavage structure (**3** in Scheme 1). In their calculations, both O_1 and O_2 of EC are coordinated to Li^+, which seems to stabilize the C_C-O_2 bond cleavage structure. However, their structure is rather artificial and does not appear in our explicit solvent model because three other ECs coordinate to Li^+. These surely verify the necessity of the present type of full DFT-MD analysis. The conclusion about 1e reduction of EC is that the bond cleavage likely occurs in the C_E-O_2 bond and a solvated EC is decomposed to **2** in Scheme 1, o_E-EC^- being the EC anion radical (see also Figure 1c). The preference of C_E-O_2 bond breaking via reduction is consistent with the results of previous studies.[21,32]

Next, we investigated the two possible paths of 1e reductive decomposition of VC (paths (3) and (4) in Scheme 1). The distances C_E-O_2 and C_C-O_2 were used as the constraints, ξ, for the paths (3) and (4), respectively. We used the supercell with and without a Li atom to clarify the effect of the VC coordination to Li^+. The resultant free energy profiles are shown in Figure 3b. The free energies at distances of 1.4 Å (equilibrium bond distance of C_E-O_2) and 1.5 Å (equilibrium bond distance of C_C-O_2) were set as the zero reference energy for C_E-O_2 (3) and C_C-O_2 (4) bond-breaking, respectively.

On the reaction path (3), the activation and reaction energies were estimated to be 15.8 (12.8) kcal/mol and −3.6 (−5.3) kcal/mol, respectively, for VC coordinated to Li^+ (uncoordi-

nated VC). The rather high activation barrier as well as the small gain in the reaction free energy indicates a lower probability of breaking of this bond. The difference between the coordinated and uncoordinated VC can be explained by the energy difference from the product. With respect to this energy reference, the barrier energies are similar for both types of VC because the C_E-O_2 bond being broken is rather away from O_1 that is responsible for the coordination to Li^+. In contrast, the reactant energy of the coordinated VC is lower than that of the uncoordinated VC. The VC anion reactant before decomposition has a singly occupied molecular orbital (SOMO) on the π^* orbital of the CO_3 moiety. This SOMO is stabilized by coordination to Li^+. The orbital energy is −2.81/−2.57 eV in the DFT cluster calculations with/without Li^+, respectively (see Supporting Information Figure S2). Thus, the barrier from the reactant looks higher in the case of VC coordinating to Li^+.

Calculations along the reaction path (4) show that the other unconstrained C_C-O_2 bond dissociates when the constrained C_C-O_2 distance is about 1.8 Å and the activation free energy is around 5 kcal/mol. The calculations indicate VC decomposition into CO and $OCHCHO^-$ (d_{CO}-VC^-; see Figure 1d). Thus, the free energy profile was not completed via the Blue-moon ensemble method. On the other hand, normal DFT-MD simulations with different initial conditions provide three different metastable products. Figure 4 shows their representa-
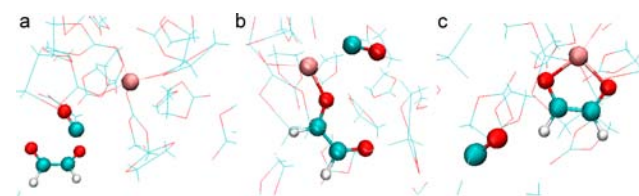

Figure 4. Snapshots of metastable VC decomposition products of path (4b) in Scheme 1 with different coordination. Intact EC molecules are shown as wireframes. Cyan, white, red, and pink spheres denote C, H, O, and Li atoms/ions, respectively.

tive configurations: (a) d_{CO}-VC^- that is apart from Li^+, (b) d_{CO}-VC^- coordinated to Li^+ by an oxygen atom, and (c) d_{CO}-VC^- coordinated to Li^+ via their two oxygen atoms. The average reaction energies with respect to the initial are −21.8, −12.6, and −23.3 kcal/mol, respectively. All the pathways indicate the release of CO gas from the Li^+ solvation shell, consistent with the experiments. Consequently, the VC reductive decomposition pathway is expected to be through the cleavage of C_C-O_2 bond (Scheme 1, path (4b)). The most probable product is likely to be configuration (c) in Figure 4, whose reaction energy is also shown in Figure 3b. These ensure that path (4b) is sufficiently exothermic.

Comparing the activation free energies between paths (3) and (4), we concluded that path (4) is preferred in the 1e reductive decomposition of VC. This conclusion is supported by comparison of the reaction free energies as well. Some previous quantum chemical studies have focused on the C_E-O_2 dissociation in VC, which turns out to be wrong, indicating the importance of DFT-MD analysis with explicit solvation shells. Note that the fragility of the C_C-O_2 bond in VC molecule was already suggested in ref 26.

We have thoroughly investigated 1e reductive decomposition of EC and VC, and suggest that an EC anion molecule can transform into an o_E-EC^- radical, and that a d_{CO}-VC^- radical with CO molecule are produced from VC. Due to the C_E-C_E

single bond, the EC anion molecule has a large structural freedom to release the internal strain at the cleavage of a C_E–O_2 bond. Simultaneously the SOMO, originally occupying the π^* orbital of the CO_3 moiety, moves to a nonbonding orbital, decreasing the instability. In contrast, the VC anion molecule has strong π conjugation on the O_2–C_E–C_E–O_2 moiety. Preference for this conjugation will make the C_c–O_2 bond breaking favorable. A detailed cluster analysis is described in the Supporting Information.

In contrast, it is known that C_2H_4 and CO are detected from EC, and CO_2 is the main reductive decomposition product in the presence of VC, though substantial amounts of CO gas are also released.[15] The results so far cannot reproduce the production of these gases. In order to clarify the origin, we have investigated the subsequent reactions after 1e reductive reaction of 2e reductive decomposition and radical reactions below.

3.3. Two-Electron (2e) Reductive Decomposition Reaction.
We next examined the 2e reductive decomposition of EC and VC. In fact, Leung recently pointed out that 2e reduction induces a process essential to the formation of SEI for the EC system.[31]

We added an excess electron to six randomly chosen configurations in the trajectory of the 1e reduction EC system with one Li atom and carried out DFT-MD sampling. Three of the initial configurations started from undecomposed EC^- (**1** in Scheme 1) and the other three do from o_E-EC^-. The 2e reduced EC was decomposed immediately within 0.2 ps in all cases. Among the undecomposed EC^- cases, two cases showed EC decomposition into CO and OCH_2CH_2O (Figure 5a); the
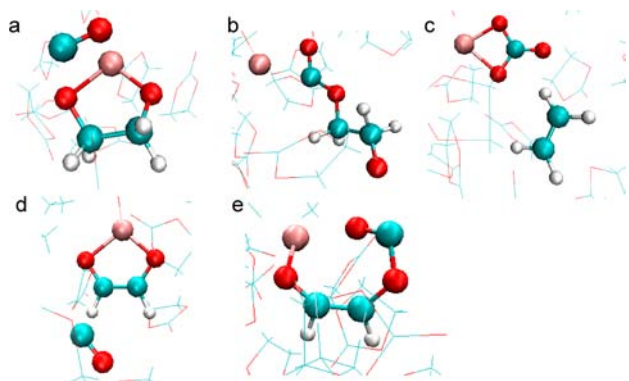
Figure 5. Snapshots of two-electron reductive decomposition products with different coordination. Intact EC molecules are shown as wireframes. Cyan, white, red, and pink spheres denote C, H, O, and Li atoms/ions, respectively. (a,b) The reactant is undecomposed EC^-, **1**. (c) The reactant is o_E-EC^-, **2**. (d,e) The reactant is undecomposed VC^-, **4**.

other indicated the dissociation of the C_c–O_2 bond (Figure 5b). In contrast, in the o_E-EC^- initial configuration cases, all three o_E-EC^- were decomposed into CO_3^{2-} and C_2H_4 (Figure 5c). Thus, the production of C_2H_4 and CO_3^{2-} mainly observed in the experiments was confirmed to occur through the 2e reduction of an EC molecule, which is consistent with a previous DFT-MD study.[32]

In the VC case, we added an excess electron to five randomly chosen configurations from the 1e reduction trajectory of the EC/VC system with one Li^+ and resumed DFT-MD simulations. All of the initial configurations started from undecomposed VC^-. In four cases, VC was decomposed into CO and d_{CO}-VC^{2-}, and in one case, it became a ring-opening

structure with C_c–O_2 bond cleavage (Figure 5e) in the 5 ps simulations. The production of CO and d_{CO}-VC^{2-} is the same as the results in the 1e reductive VC decomposition, and 2e reductive decomposition does not reproduce the CO_2 gas production yet.

3.4. Anion Radical Attack to Nearby Intact Molecule.
As shown in the previous section, the mechanism of CO_2 evolution observed in the presence of VC is still an open question. We then considered another possibility, attack of an anion radical generated by the 1e reduction to a neutral intact molecule nearby in the electrolyte. Possible processes are summarized in Scheme 2. We carried out DFT-MD simulations under the 1e reduction condition for these reactants and products and examined the stability based on the average total energies.

Scheme 2. Possible Interactions between Intact EC (1) and VC (4) Molecules with the EC (2) and VC (6b) Decomposed Anion Radicals
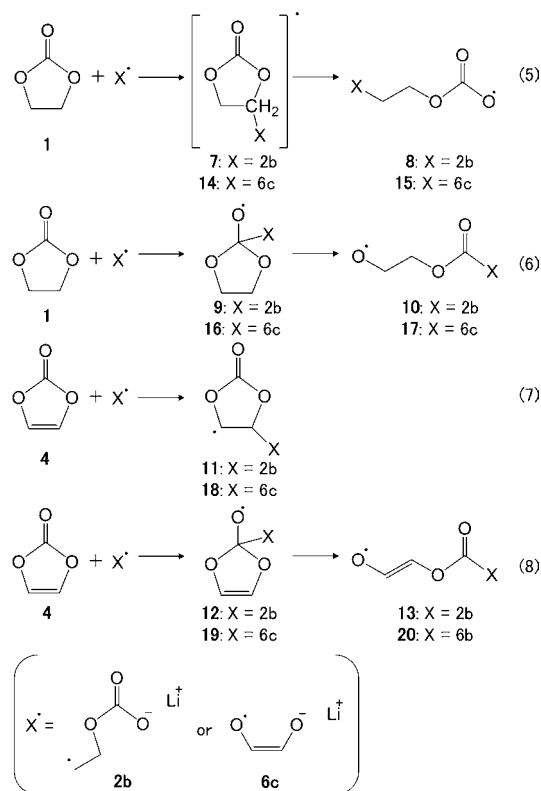
Starting the DFT-MD simulations from the intermediate state of path (5), we found spontaneous separation between the intact EC and the radicals (o_E-EC^- or d_{CO}-VC^-). C_E with sp³ bonding in the intact EC seemed inactive against the ring-opening. The same tendency is obtained in path (6), where the radical attacks on the C_c site of the intact EC. The o_E-EC^- attack is an endothermic reaction, and the d_{CO}-VC^- attack reaction did not proceed because of the spontaneous separation of the reactants.

In the case of path (7), the binding of intact VC with d_{CO}-VC^- showed spontaneous separation. This result indicates that oligomerization of the decomposed VC anion radical is not energetically very favorable. In contrast, the radical attack of o_E-EC^- to the C_E site in the intact VC has a reaction energy of −34.9 kcal/mol, which is significantly exothermic. Similar

tendency was also observed in path (8). Spontaneous separation from the intermediate state **19** was observed in the case of the VC radical attack, whereas ring-opening was found to be exothermic (−18.5 kcal/mol) in the case of EC radical attack to the C_c site in the intact VC.

The product of path (7) could possibly generate CO_2 through a reverse Diels−Alder reaction of path (9) in Scheme 3, as noted by Wang et al.[8] However, Wang et al. considered

Scheme 3. Possible Subsequent Reaction after the Radical Attack of o_E-EC$^-$ on VC for CO_2 Evolution
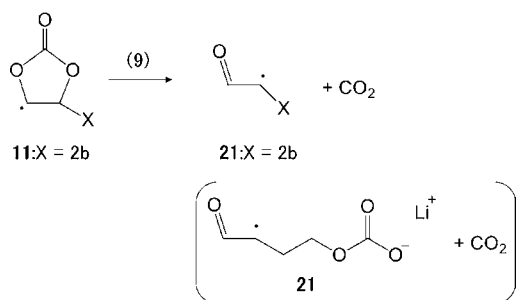
the CO_2 generation from the intermolecular reaction between VC and the VC anion radical opened through the C_E-O_2, **5**. But we have already shown that C_E−O_2 bond cleavage to be less likely to occur for the VC decomposition radical (6b). Therefore, we have dealt with the reaction between the intact VC, **2**, and o_E-EC$^-$. We examined the free energy profile of the binding with the Blue-moon ensemble technique, as indicated in Figure 6a. We used the sum of the distances of two cleaved bond, i.e., C_C−O_2 and C_E−O_2 as a constraint. The zero reference energy is defined when the sum of the bond distance was 2.9 Å, based on the equilibrium bond distances of C_C−O_2 (1.5 Å) and C_E−O_2 (1.4 Å). The activation free energy and the reaction free energy were estimated to be 9.7 and −16.2 kcal/

mol, respectively. Though the barrier is a little bit high, this process is reasonably probable in practice.

Figure 6b displays the average of the bond distances of VC when o_E-EC$^-$ attacks to intact VC. We found that the C_E−O_2 bond of VC is dissociated first and the dissociation of far-side C_C−O_2 then follows. As another case, attack of undecomposed VC$^-$, **4** in Scheme 2, to C_E site of the intact VC can generate CO_2 through the path (S1) (see Supporting Information Scheme S1). The CBC calculations also show the same results. Yet we expect that the reaction between VC anion and intact VC is unlikely to occur at the only a few weight % of VC additives in the EC solvent. We therefore conclude that a radical anion attack at the C_E site of VC is a most probable reaction path that can generate CO_2.

3.5. Discussion. We summarize the gaseous products of the reductive decompositions of EC and EC/VC systems on the basis of our calculations and compare our results with the experimental observation. Our EC systems indicated that C_2H_4 and CO evolution occurs mainly through the 2e reductive decomposition of EC. This result supports the conclusion of recent theoretical works by Leung et al.[31,32] and is also consistent with C_2H_4 and CO observation in the VC-free EC electrolyte in a gas chromatography experiment.[15] Note that binding of the EC anion radical o_E-EC$^-$ is also a possibility for C_2H_4 evolution.

When VC was added in the electrolyte, the total amount of generated C_2H_4 significantly decreased compared to the VC-free electrolyte case. On the other hand, a certain amount of CO_2 evolved with addition of VC.[15] Our results indicate that CO_2 evolution occurs mainly through the attack of an EC anion radical made by 1e reduction to the C_E site of an intact VC. The large exothermic reaction energy suggests that this reaction may be reasonably faster. Therefore, consumption of the EC radicals by this process may suppress the 2e reduction of the EC solvent causing the C_2H_4 evolution. If the SEI film grows on the electrode, the 2e reduction is more suppressed, and CO_2 evolution via the present 1e mechanism will be more dominant.

It is widely accepted that VC is a "sacrificial reduction additive", and VC anion radical after 1e reduction can trigger the subsequent reaction.[10,22] The present results suggest a completely different mechanism from this scenario. Before reduction, it is energetically favored that Li$^+$ is coordinated by four EC molecules and VC is uncoordinated. When one excess electron is introduced, this electron may transfer to the uncoordinated VC. However, the solvation shells of $(EC)_3(EC^-)Li^+$ and $(EC)_3(VC^-)Li^+$ are thermodynamically favorable. This suggests two possibilities, that the excess electron on the uncoordinated VC transfers to an EC molecule coordinating to Li$^+$ and that the VC anion itself migrates into the solvation shell. Furthermore, taking into account that there are only a few weight percent of VC additives in the electrolyte, one cannot assume that VC is always reductively decomposed before EC. Thus, a certain amount of EC anion radicals coordinating to Li$^+$ is expected in practice, and the VC additive preferentially reacts with this EC anion radical. This suppresses the 2e reduction of EC as well as the binding of the EC radicals, while enhancing the evolution of CO_2 molecules. This may lead to a better quality of SEI films.

We also discuss the role of VC in the decrease of the initial irreversible capacity. The initial irreversible capacity corresponds to the total amount of charge expended for the SEI formation reaction. For this reason, 2e reduction per one molecule to form SEI is disadvantageous compared to the 1e
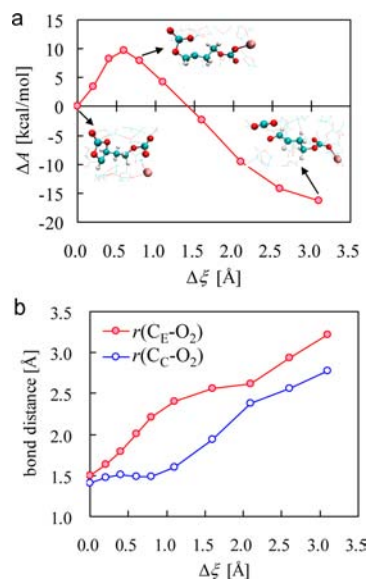

Figure 6. (a) Free energy change, ΔA, of path (9) along the mechanical constraint $\Delta \xi = r(C_E-O_2) + r(C_C-O_2) - (r_{eq}(C_E-O_2) + r_{eq}(C_C-O_2))$, where r_{eq} is the equilibrium bond distance. (b) Bond distance variation in path (9) with respect to the mechanical constraint $\Delta \xi$.

reduction. If the radical molecule reacts with VC, and if its product also reacts with a neutral molecule to form polymerized SEI, then, the total amount of charge used for the SEI formation reaction will significantly decrease.

In contrast, if the reductive VC decomposes into CO and d_{CO}-VC$^-$, the d_{CO}-VC$^-$ cannot react with another intact molecule (VC, EC in the solvent) and would not contribute to the effective SEI formation, as previously mentioned. Once the amount of VC increases, the VC reduction process will begin to increase, and the intermolecular reaction will decrease. It will then become impossible for VC molecules to play a role in the SEI formation. This implies that the VC reductive decomposition prevents making the source of SEI formation through the acceptance of EC radicals. The reductive decomposition pathways discussed in this work are schematically summarized in Figure 7.
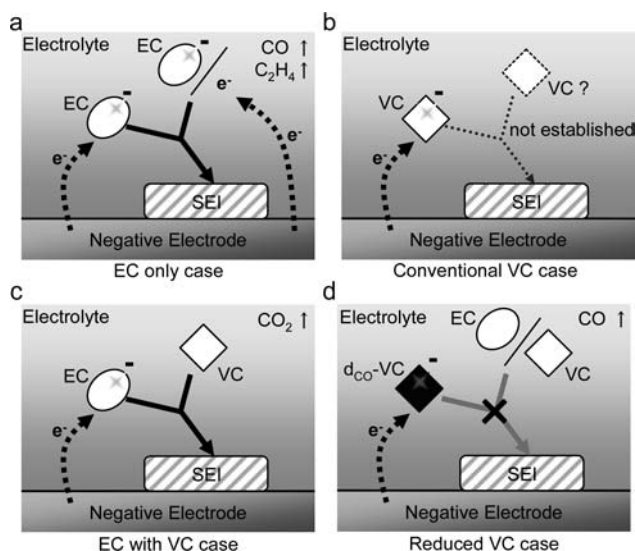

Figure 7. Schematic summary of the reductive reactions of the EC and EC/VC systems. (a) EC only case: EC radical oligomerization following 2e reduction will be the source of SEI.[21,31] (b) A conventional pathway for the EC/VC system, namely oligomerization of VC anion radical sacrifically reduced. (c) A new mechanism with 1e reduction only for the EC/VC system, proposed in this work. VC passivates the EC anion radical. (d) Possible case with reductively decomposed VC. The product d_{CO}-VC$^-$ is not reactive so that it may need another electron or another reduced molecule for the subsequent reactions.

Finally, we note the dependence on the exchange correlation functional by comparing the DFT-MD simulation results with those of the CBC calculations using PBE as pure-DFT and B3LYP as hybrid-DFT. The activation energies and the reaction energies are found quite comparable between these calculations, in agreement within 5 kcal/mol difference (see Supporting Information Tables S3 and S4). Thus, the conclusions based on the present DFT-MD simulations will not alter qualitatively, depending on the functionals.

4. CONCLUSIONS

We have investigated the thermodynamics and the kinetics of reductive decomposition of the EC solvent only and the EC solvent with the VC additive to elucidate the additive effect on the initial process of SEI formation. We used standard DFT-MD sampling with explicit solvent for the equilibrium states

and the Blue-moon ensemble technique for free energy profiles of the reactions.

We found that 1e reduction induces breaking of the C_E–O_2 bond in EC to produce o_E-EC$^-$, while d_{CO}-VC$^-$ and CO are generated from VC through C_C–O_2 bond breaking, in contrast to a previous study.[22] When another electron is added to the system (2e reduction), EC decomposition produces CO_3^{2-} + C_2H_4 or CO + alkylcarbonate, whereas CO production occurs again at the 2e reduction of VC. We then examined the attack of anion radical made by 1e reduction to the nearby intact molecule and found that the EC radical attack to the intact VC enhances the CO_2 production. These mechanisms on the atomic scale are in good agreement with the experimental observations of the gaseous products. Contrary to the conventional scenario that VC additive is sacrificially reduced and makes a VC oligomer that seeds SEI formation, the present results provide a completely different mechanism: the VC additive preferentially reacts with the EC anion radical to suppress the 2e reduction of EC, the main initial stage of SEI formation in the VC-free EC electrolyte. Because this VC mechanism is realized via 1e reduction, the irreversible capacity at the SEI formation will decrease as well, which is also consistent with the experiments. These results not only reveal the primary role of the VC additive in the EC solvent but also provide a new fundamental perspective for the reductive decomposition of carbonate-based electrolyte near the negative electrode.

■ ASSOCIATED CONTENT

ⓢ Supporting Information

Properties of solvation shells and electron affinities of the EC and EC/VC systems, detailed cluster analysis of decomposition, two Li$^+$ coordination, and anion radical attack under one electron reduction conditions. This material is available free of charge via the Internet at http://pubs.acs.org.

■ AUTHOR INFORMATION

Corresponding Author
yukihiro_okuno@fujifilm.co.jp; tateyama.yoshitaka@nims.go.jp
Notes
The authors declare no competing financial interest.

■ ACKNOWLEDGMENTS

■ REFERENCES

(1) Armstron, A. R.; Bruce, P. G. *Nature* **1996**, *381*, 499−500.
(2) Tarascon, J.-M.; Armand, M. *Nature* **2001**, *414*, 359−367.
(3) Chen, Y.; Freunberger, S. A.; Peng, Z.; Bardé, F.; Bruce, P. G. *J. Am. Chem. Soc.* **2012**, *134*, 7952−7957.
(4) Kinoshita, S.; Kotato, M.; Sakata, Y.; Ue, M.; Watanabe, Y.; Morimoto, H.; Tobisima, S. *J. Power Sources* **2008**, *183*, 755−760.

(5) Tavassol, H.; Buthker, W.; Ferguson, G. A.; Curtiss, L. A.; Gweirth, A. A. *J. Electrochem. Soc.* **2012**, *159*, A730−A738.

(6) Seo, D. M.; Borodin, O.; Han, S.-D.; Boyle, P. D.; Henderson, W. A. *J. Electrochem. Soc.* **2012**, *159*, A1489−A1500.

(7) Bryantsev, V. S.; Blanco, M. *J. Phys. Chem. Lett.* **2011**, *2*, 379−383.

(8) *Lithium-ion batteries: solid-electrolyte interphase*; Wang, Y., Balbuena, P. B., Eds.; Imperial College:London, 2004.

(9) Aurbach, D. *J. Power Sources* **2000**, *89*, 206−218.

(10) Zhang, S. S. *J. Power Sources* **2006**, *162*, 1379−1394.

(11) Jehoulet, C.; Biensam, P.; Bodet, J. M.; Broussely, M.; Moteau, C.; Tessier-Lescourret, C. *Proc. Electrochem. Soc* **1997**, *97−18*, 974−985.

(12) Yoshida, H.; Fukunaga, T.; Hazama, T.; Terasaki, M.; Mizutani, M.; Yamachi, M. *J. Power Sources* **1997**, *68*, 311−315.

(13) Ogumi, Z.; Sano, A.; Inaba, M.; Abe, T. *J. Power Sources* **2001**, *97−98*, 156−158.

(14) Aurbach, D.; Gamolsky, K.; Markovsky, B.; Gofer, Y.; Schmidt, M.; Heider, U. *Electrochim. Acta* **2002**, *47*, 1423−1439.

(15) Ota, H.; Sakata, Y.; Inoue, A.; Yamaguchi, S. *J. Electrochem. Soc.* **2004**, *151*, A1659−A1669.

(16) Ota, H.; Sakata, Y.; Otake, Y.; Shima, K.; Ue, M.; Yamaki, J. *J. Electrochem. Soc.* **2004**, *151*, A1778−A1788.

(17) Zhang, X.; Pugh, J. K.; Ross, P. N., Jr. *Electrochem. Solid-State Lett.* **2001**, *4*, A82−A84.

(18) Zhuang, G. V.; Xu, K.; Yang, H.; Jow, T. R.; Ross, P. N., Jr. *J. Phys. Chem. B* **2005**, *109*, 17567−17573.

(19) Onuki, M.; Kinoshita, S.; Sakata, Y.; Yanagidate, M.; Otake, Y.; Ue, M.; Deguchi, M. *J. Electrochem. Soc.* **2008**, *155*, A794−A797.

(20) Ouatani, L.; Dedryvère, R.; Siret, C.; Biensan, P.; Reynaud, S.; Iratcabal, P.; Gonbeau, D. *J. Electrochem. Soc.* **2009**, *156*, A103−A113.

(21) Wang, Y. X.; Nakamura, S.; Ue, M.; Balbuena, P. B. *J. Am. Chem. Soc.* **2001**, *123*, 11708−11718.

(22) Wang, Y.; Nakamura, S.; Tasaki, K.; Balbuena, P. B. *J. Am. Chem. Soc.* **2002**, *124*, 4408−4421.

(23) Wang, Y.; Balbuena, P. B. *J. Phys. Chem.* **2002**, *106*, 4486−4495.

(24) Li, T.; Balbuena, P. B. *J. Electrochem. Soc.* **1999**, *146*, 3613.

(25) Marquez, A. *Mater. Chem. Phys.* **2007**, *104*, 199−209.

(26) Han, Y.-K.; Lee, S. U.; Ok, J.-H.; Cho, J.-J.; Kim, H.-J. *Chem. Phys. Lett.* **2002**, *360*, 359−366.

(27) Han, Y.-K.; Lee, S. U. *Bull. Kor. Chem. Soc.* **2005**, *26*, 43−46.

(28) Bhatt, M. D.; Cho, M.; Cho, K. *J. Solid State Electrochem.* **2012**, *16*, 435−441.

(29) Masia, M.; Probst, M.; Rey, R. *J. Phys. Chem. B* **2004**, *108*, 2016−2027.

(30) Tasaki, K. *J. Phys. Chem. B* **2005**, *109*, 2920−2933.

(31) Leung, K. *Chem. Phys. Lett.* **2013**, *568−569*, 1−8.

(32) Leung, K.; Budzien, J. L. *Phys. Chem. Chem. Phys.* **2010**, *12*, 6583−6586.

(33) Yu, J.; Balbuena, P. B.; Budzien, J.; Leung, K. *J. Electrochem. Soc.* **2011**, *158*, A400−A410.

(34) Leung, K.; Qi, Y.; Zavadil, K. R.; Jung, Y. S.; Dillon, A. C.; Cavanagh, A. S.; Lee, S.-H.; George, S. M. *J. Am. Chem. Soc.* **2011**, *133*, 14741−14754.

(35) Leung, K. *J. Phys. Chem. C* **2012**, *116*, 9852−9861.

(36) Ganesh, P.; Kent, P. R. C.; Jiang, D. *J. Phys. Chem. C* **2012**, *116*, 24476−24481.

(37) Car, R.; Parrinello, M. *Phys. Rev. Lett.* **1985**, *55*, 2471.

(38) CPMD, http://www.cpmd.org/, copyright IBM Corp. 1990−2008, copyright MPI für Festkörperforschung Stuttgart 1997−2001.

(39) Nose, S. *J. Chem. Phys.* **1984**, *81*, 511−519. Hoover, W. G. *Phys. Rev. A* **1985**, *31*, 1695−1697.

(40) Goedecker, S.; Teter, M.; Hutter, J. *Phys. Rev. B* **1996**, *54*, 1703−1710.

(41) Hartwigsen, C.; Goedecker, S.; Hutter, J. *Phys. Rev. B* **1998**, *56*, 3641−3662.

(42) Krack, M. *Theor. Chem. Acc.* **2005**, *114*, 145−152.

(43) Sprik, M.; Ciccotti, G. *J. Chem. Phys.* **1998**, *109*, 7737−7744.

(44) Frisch, M. J.; Trucks, G. W.; Schlegel, H. B.; Scuseria, G. E.; Robb, M. A.; Cheeseman, J. R.; Scalmani, G.; Barone, V.; Mennucci, B.; Petersson, G. A.; Nakatsuji, H.; Caricato, M.; Li, X.; Hratchian, H. P.; Izmaylov, A. F.; Bloino, J.; Zheng, G.; Sonnenberg, J. L.; Hada, M.; Ehara, M.; Toyota, K.; Fukuda, R.; Hasegawa, J.; Ishida, M.; Naka-jima, T.; Honda, Y.; Kitao, O.; Nakai, H.; Vreven, T.; Montgomery, Jr., J. A.; Peralta, J. E.; Ogliaro, F.; Bearpark, M.; Heyd, J. J.; Brothers, E.; Kudin, K. N.; Staroverov, V. N.; Kobayashi, R.; Normand, J.; Ragha-vachari, K.; Rendell, A.; Burant, J. C.; Iyengar, S. S.; Tomasi, J.; Cossi, M.; Rega, N.; Millam, J. M.; Klene, M.; Knox, J. E.; Cross, J. B.; Bak-ken, V.; Adamo, C.; Jaramillo, J.; Gomperts, R.; Stratmann, R. E.; Yazyev, O.; Austin, A. J.; Cammi, R.; Pomelli, C.; Ochterski, J. W.; Martin, R. L.; Morokuma, K.; Zakrzewski, V. G.; Voth, G. A.; Salvador, P.; Dannenberg, J. J.; Dapprich, S.; Daniels, A. D.; Farkas, Ö.; Fores-man, J. B.; Ortiz, J. V.; Cioslowski, J.; Fox, D. J. *Gaussian 09*, Revision A.2; Gaussian, Inc.: Wallingford, CT, 2009.

(45) Becke, A. D. *J. Chem. Phys.* **1993**, *98*, 5648−5652.

(46) Peredew, J. P.; Burke, K.; Ernzerhof, M. *Phys. Rev. Lett.* **1996**, *77*, 3865−3868.

(47) Peredew, J. P.; Burke, K.; Ernzerhof, M. *Phys. Rev. Lett.* **1997**, *78*, 1396.